Simplified Thermal Model of Disk-Shaped Automotive Smart Braking Actuators

Simplified Thermal Model of Disk-Shaped Automotive Smart Braking Actuators

Federica Graffeo, *Student Member,IEEE*
Politecnico di Torino
Dipartimento di Energia
Turin, Italy
federica.graffeo@polito.it

Silvio Vaschetto, *Senior Member, IEEE*
Politecnico di Torino
Dipartimento di Energia
Turin, Italy
silvio.vaschetto@polito.it

Alessio Miotto
Brembo S.p.A.
Advanced R&D
Curno, Italy
alessio_miotto@brembo.it

Fabio Carbone
Brembo S.p.A.
Advanced R&D
Curno, Italy
fabio_carbone@brembo.it

Alberto Tenconi, *Senior Member, IEEE*
Politecnico di Torino
Dipartimento di Energia
Turin, Italy
alberto.tenconi@polito.it

Emmanuel Agamloh, *Senior Member, IEEE*
Dept. of Electrical and Computer Engineering
Baylor University
Waco, Texas, USA
emmanuel_agamloh@baylor.edu

Andrea Cavagnino, *Fellow, IEEE*
Politecnico di Torino
Dipartimento di Energia
Turin, Italy
andrea.cavagnino@polito.it

***Abstract*— This paper articulates the challenges in the thermal modelling of surface-mounted permanent magnet motors for automotive brake-by-wire systems, which operate by injecting high dc currents in two of the three phases for short time intervals. This unconventional operation requires dedicated thermal models for the prediction of uneven heat distributions inside the machine. This study extends a previous work conducted on slender-shaped motors to a disk-shaped machine where the edge effects could compromise the model accuracy. Additionally, here efforts have been made to minimize the number of experimental tests needed for the correct calibration of the proposed phase-split lumped-parameters thermal models.**

Keywords—PM synchronous machines; thermal models; brake-by-wire actuators; lumped-parameters thermal network (LPTN); phase-split LPTN, aspect ratio

I. INTRODUCTION

In recent years, the automotive industry has witnessed a massive replacement of traditional mechanical systems with electrified smart actuators. In this perspective, the brake-by-wire (BBW) systems represent a step in this direction. The BBW offers a lot of advantages in comparison to its traditional counterpart. It can achieve a faster response time which reduces the braking distance. Lower maintenance is required thanks to the wear monitoring and the reduction of the required brake fluid. Its flexible layout makes it suitable for different vehicles. Furthermore, its potential integration with energy recovery systems can actively contribute to vehicle energy management strategies [1]-[3].

The electric motor of the BBW systems generally operates under unconventional and severe working conditions, which consist of injecting high *dc* currents in two of the three phases for short time intervals. This causes an uneven heat distribution in the machine, which can lead to premature ageing of the machine insulation and compromising its correct functioning and exploitation [4]-[7]. Hence, it is necessary to develop thermal models able to estimate the actual winding temperatures during operations, but also sufficiently simple to allow their potential future application in the drive control system for real-time temperature monitoring and prediction [8].

This last constrain makes the lumped-parameters thermal networks (LPTNs) the most effective way to predict the motor temperatures. A well calibrated LPTN allows to reach solid and reliable results [9]. Moreover, these low-order thermal models are fast in solving and discard all the information that is not useful for the final application. On the contrary, finite elements software and computational fluid dynamics tools generally require a long computational time that often discourages their use in real-time predictions [10].

In this paper, the LPTN approach is used to predict the temperatures of the main parts of a synchronous permanent magnet (PM) motor in a BBW system. The BBW system under analysis is composed of two PM motors: one for the rear braking and one for the front braking of the vehicle. The two motors are characterized by very different aspect ratios, i.e. the ratio between the axial length L over the diameter D at the air gap. In previous work, the authors proposed dedicated phase-split LPTNs to predict the temperatures of the main parts of the motor with the highest aspect ratio, hereinafter the '*slender*' motor [8]. The proposed thermal networks were able to compute the temperature of each phase separately, allowing the prediction of the uneven thermal conditions of the motor. In this paper, the same LPTNs are applied to the motor with the lowest aspect ratio, hereinafter the '*disk-shaped*' motor. Indeed, the disk shape could compromise the accuracy of the model, as more pronounced edge effects are expected. Several thermal tests on a machine prototype are used to calibrate the thermal networks by means of the particle swarm optimization (PSO) technique [11]. The applicability of the resulting LPTNs for the *disk-shaped* motor is validated over two different load cycles performed in two different ambient conditions: ambient air and climatic chamber. The latter is the most representative of the actual BBW working conditions as the temperature of the chamber is set at the expected operating temperature of the system. Finally, a sensitivity analysis related to the minimum number of thermal tests to be performed to obtain satisfactory thermal parameters is presented. This implies the minimization of the computational time required by the optimization process.

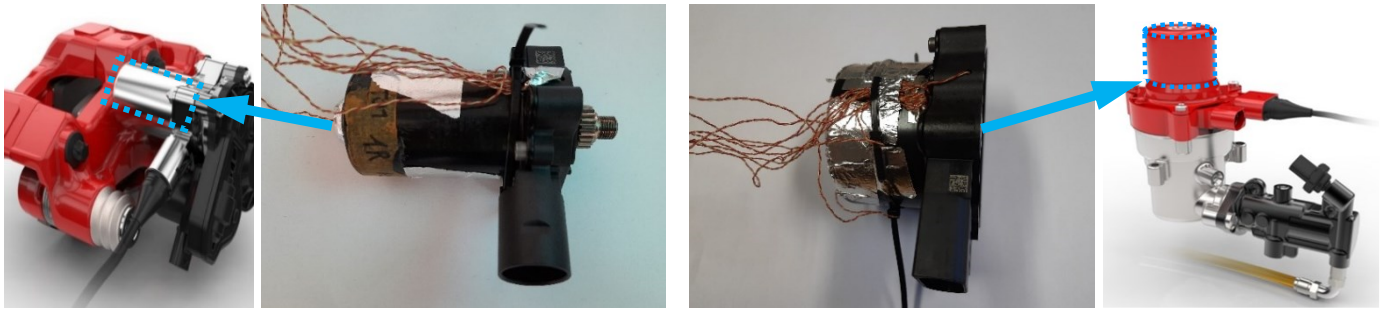

(a) (b)

Fig.1 The PM motors for the considered BBW system and their positioning inside the actuators [3]:(a) *slender* motor, (b) *disk-shaped* motor.

II. THE MOTORS UNDER TESTS

A. The slender and the disk-shaped motors

Fig. 1 shows the PM synchronous motors under test. In particular, Fig. 1a shows the *slender* motor, and Fig. 1b the *disk-shaped* motor. These machines equip the two different systems shown on the sides of Fig. 1. The structure on the left is an electromechanical brake caliper in which electric energy is directly converted into clamping force, while the structure on the right side is an electro-hydraulic actuator that converts electric energy into hydraulic pressure on a standard brake caliper. The two machines are PM motors, rated a few hundred watts, with a star-connected concentrated winding. The *disk-shaped* motor features a rated power 1.5 times greater than the *slender* motor, and a lower aspect ratio: $L / D = 0.42$ for the *disk-shaped* motor, $L / D = 1.69$ for the *slender* motor. In their normal working conditions, the machines are low voltage supplied and repetitive pulses of *dc* currents are injected in two of the three phases. This results in an asymmetrical location of the heat sources and, consequently, in uneven temperature distributions inside the machines. An extensive thermal test campaign has been conducted on both motors for the calibration of the thermal networks.

B. The performed thermal tests

The two motors have been equipped with several thermocouples – see Fig. 1 – and tested in two different ambient conditions: ambient air and climatic chamber. Inside the climatic chamber, the ambient temperature was set to 120°C to considerate the operating temperature of the BBW system. In the real working conditions, the two supplied phases are randomly selected. In the performed thermal tests, the two supplied phases were chosen to be always the same to consider the worst-case scenario. The test campaign was based on three different kinds of thermal tests: '*steady state*', '*pulse-current*' and '*load cycle*' tests. The first consists of injecting a *dc* current until the steady-state conditions are reached, see Fig. 2a. The second consists of injecting a *dc* current until the maximum admissible temperature (180°C) is reached, as depicted in Fig. 2b. The cooling of the steady-state and pulse-current tests is carried out with a current value of 20A. The third consists of injecting repetitive current pulses with the aim of testing the motor under working conditions similar to the real ones. Two load cycle tests have been defined. The load cycle 1 consists of injecting repetitive pulses of *dc* currents for a defined time duration; subsequently, another defined time interval is waited before the next pulse of current.

For the second load cycle, two different values of currents are injected. The lower value is injected 5 consecutive times before supplying the motor with one pulse of the highest current. In the following periods, the number of low current injections progressively decreases by one, as shown in Fig. 2c.

Details on the test campaign conducted on the *slender* motor are discussed in [8], while the thermal tests performed on the *disk-shaped* motor are the followings:

- n.1 steady-state test in ambient air, conducted injecting 50 A;
- n.1 steady-state test in the climatic chamber, conducted injecting 40 A;
- n.3 pulse-current tests in ambient air, from 80 A up to 120 A with a current step of 20A;
- n.8 pulse-current tests in the climatic chamber, from 50 A up to 120 A with a current step of 10A;
- n.2 load cycle tests in the ambient air;
- n.2 load cycle tests in the climatic chamber.

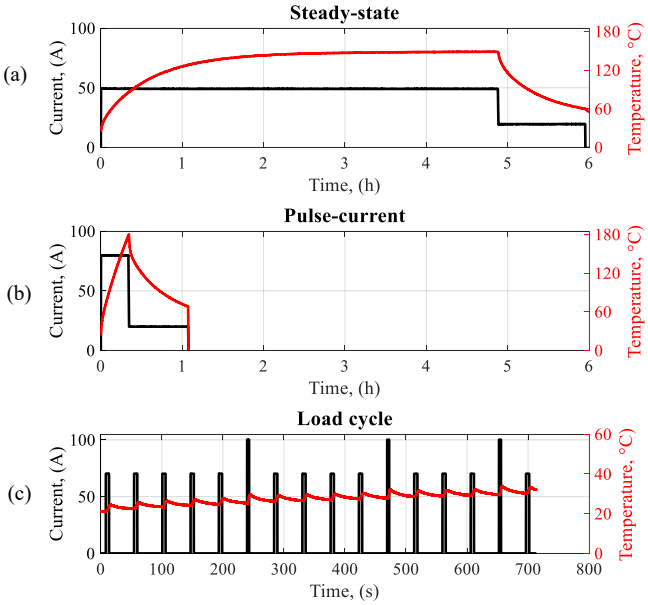

Fig.2 The performed thermal tests:
(a) steady-state, (b) pulse-current, (c) load cycle.

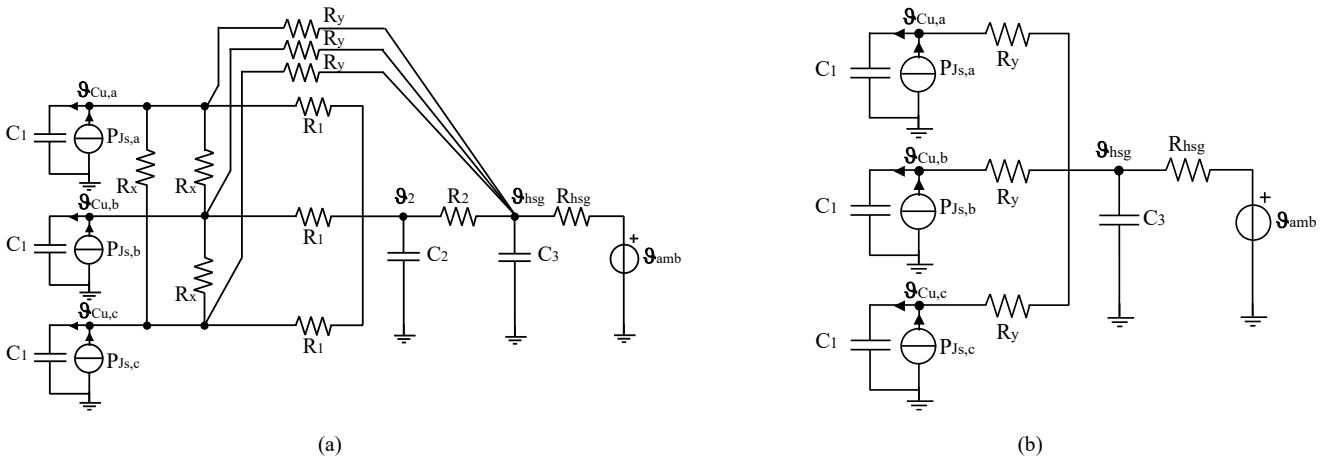

Fig.3 The proposed phase-split LPTNs: (a) the *complete* thermal model and (b) the *simplified* LPTN.

III. THE PROPOSED PHASE-SPLIT THERMAL NETWORKS

The proposed phase-split LPTNs were initially calibrated and tested on the *slender* motor [8]. These models are shown in Fig. 3, where the three phases were split into three branches to independently model the thermal behaviour of each phase winding. In the '*complete'* LTPN of Fig. 3a the thermal resistance R_x models the heat exchange among the three phases, R_y models the heat path between the end windings and the housing and R_1 the heat path between the stator winding in the slot and the stator back iron. Finally, R_2 is the thermal resistance between the stator core and the housing.

The analysis conducted on the *slender* motor led to the conclusion that the proposed thermal model could be usefully simplified to the network shown in Fig. 2b. In the '*simplified'* thermal network, R_y must be considered as an equivalent thermal resistance between each stator phase winding and the housing. In both the LPTNs, the measured ambient temperature and the injected power are used as input for the model. The latter is supposed to be equally shared by the two supplied phases. The predicted temperatures are obtained by solving the system of differential equations by means of Euler's method. The two proposed LTPNs are here used to predict the temperature of the disk-shaped motor to verify the accuracy of the model and to point out the differences between the two thermal networks.

A. Thermal parameters definition

For what concerns the thermal resistance R_{hsg} between the housing and the surrounding ambient, one steady-state test is sufficient to determine its value, as expressed in (1).

$$R_{hsg}\big|_{t\to\infty} = \frac{\theta_{housing}-\theta_{ambient}}{P}\bigg|_{t\to\infty} \qquad (1)$$

Where $\theta_{housing}$ is the temperature of the housing, $\theta_{ambient}$ is the temperature of the surrounding ambient, P is the injected power, and all variables are evaluated for $t \to \infty$, i.e. in steady-state conditions. However, the value of the housing-ambient thermal resistance is not uniquely defined for all the thermal operating conditions; indeed, it may vary due to different reasons.

The various combinations of natural convection, forced convection and radiation thermal phenomena affect the final value of R_{hsg}. Changes may also be caused by the reached housing and ambient temperatures [12].

Different ambient temperatures and thermal phenomena occurred in the tests performed in the ambient air with respect to the climatic chamber ones. Hence, two different housing thermal resistance values have been found from the steady-state tests, depending on the ambient conditions. Consequently, the analyses on the tests performed in the ambient air and in the climatic chamber will be treated separately.

For what concerns the remaining thermal parameters, the definition of practical analytical formulations for their computation is highly complex due to the unconventional supply conditions and the small geometrical dimensions of the motors. Therefore, these values are estimated by means of the particle swarm optimization technique [11]. The objective function of the optimization is the sum of the quadratic error between the measured and computed temperatures in different conditions, as expressed in (2).

$$\varepsilon = \sum_{j=1}^{n_{test}} \sum_{i=1}^{n_\vartheta} \sum_{z=0}^{Z} \left(\vartheta^{j}_{measured_{i,z}} - \vartheta^{j}_{computed_{i,z}}\right)^2 \qquad (2)$$

In this function, ε is the total quadratic error, j is the index that indicates the j-th thermal test; i is the index that indicates the temperatures of the considered machine parts (the three phases and the housing); z is the index that indicates the considered temperature samples. If the optimization process is used to also obtain the housing thermal resistance, the same values of the measurements are found. This value has been fixed to the measured one for the presented optimizations to remove the burden of optimizing an additional parameter.

The simplification of the thermal network leads to a sharp reduction of the computational time, as fewer parameters need to be optimized. For example, when 1 steady-state and 7 pulse-current temperature tests are used to determine the model parameter for the *slender* motor, the computational time reduces from one hour and a half for the *complete* LTPN to 5 minutes for the *simplified* one [8].

TABLE I - THERMAL PARAMETERS OF THE PROPOSED LPTNS FOR THE TESTS IN AMBIENT AIR.

Parameter	*Complete* LPTN	*Simplified* LPTN
C_1, (J/°C)	68	62.5
C_2, (J/°C)	$2.2 \cdot 10^6$	
C_3, (J/°C)	479.8	467.1
R_x, (°C/W)	15.4	
R_1, (°C/W)	$1.5 \cdot 10^8$	
R_2, (°C/W)	$2.2 \cdot 10^7$	
R_y, (°C/W)	1.5	1.2
R_{hsg}, (°C/W)	2.35	2.35

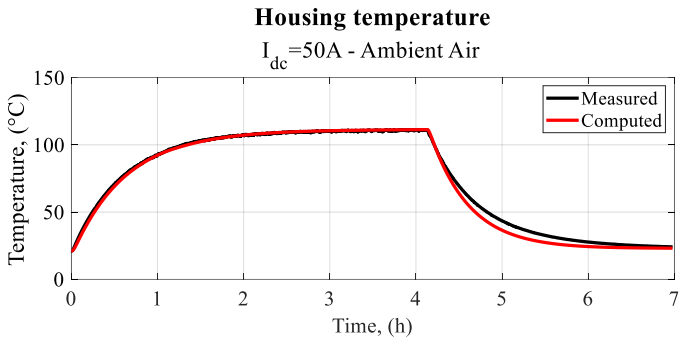

Fig.4 Computed and measured housing temperature for the steady-state test in ambient air.

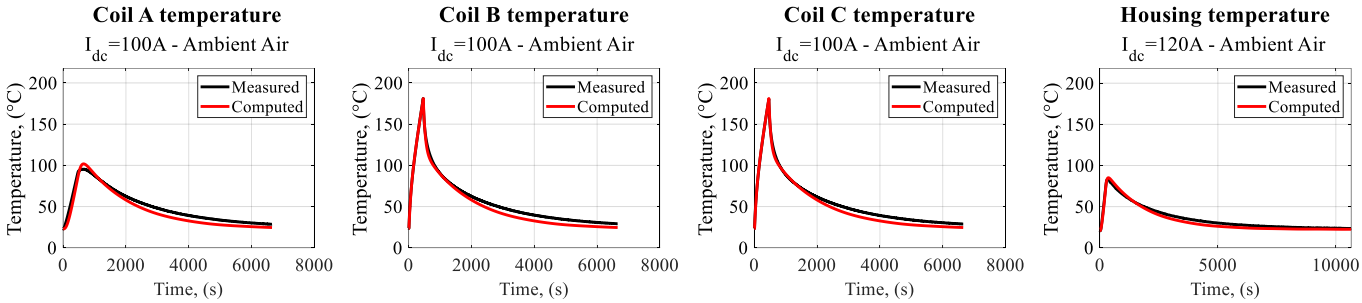

Fig.5 Measured and computed temperatures of one pulse-current test for the *simplified* LPTN.

IV. TESTS IN AMBIENT AIR FOR THE DISK-SHAPED MOTOR

The proposed LPTNs aim to predict the temperatures of the main parts of the motor during the operations. As listed in Section II, 1 steady-state and 3 pulse-current tests were performed in ambient air and used as the baseline for the optimization of the thermal parameters of both thermal networks (*simplified* and *complete*). It is reminded that the value of the housing thermal resistance comes from measurements, while all the other parameters are optimized and can vary from zero to infinite. The obtained values of the parameters for both LPTNs are listed in Table I

Regarding the *complete* thermal network, the following considerations can be drawn on the obtained parameters. A low value of the thermal resistance R_y is found in comparison to all the other thermal resistances. The values of R_1 and R_2 are practically infinite. This means that most of the heat flux does not encounter the thermal resistances R_1 and R_2 and does not reach the node θ_2, see Fig. 3a. As a consequence, the value of the thermal capacitance C_2 has no effect on the heat repartition in the thermal network. The heat flux mainly reaches the housing frame through the thermal resistance R_y. These considerations suggest the reduction of the thermal network to the *simplified* LPTN shown in Fig. 3b, where the node θ_2 is bypassed. This is also confirmed by the obtained values of the thermal parameters for the *simplified* thermal network (see Table I). Comparable values of C_1, C_3 and R_y are obtained in the two thermal networks. Similar conclusions were found in [8] for the *slender* motor. Ultimately, between the two networks, the *simplified* one achieves equally valid results but significantly reduces the computational time.

Therefore, the results of only the *simplified* LPTN are reported in the following sections.

A. Steady-state and pulse-current thermal tests

With the thermal parameters of Table I, the housing temperature of the steady-state test is well predicted by the LPTN, as depicted in Fig. 4. Good agreements with the measurements are also obtained for all the pulse-current tests. For example, Fig.5 shows the temperatures computed by the *simplified* LPTN for the pulse-current test performed by injecting a current of 100A between phase B and phase C. The difference in terms of maximum temperatures reached by the supplied phases and the one left open is well evident in Fig. 5 and the proposed thermal model accomplishes a good prediction of both values.

B. Load cycle thermal tests

The thermal networks with the thermal parameter obtained by optimization on steady-state and pulse-current tests are thus used to predict the temperature profiles of the load cycle tests. In both cycles, phase B and phase C are supplied as explained in Section II, while phase A is left open. Both phase-split thermal networks can reach a good agreement between measured and computed temperatures. The obtained results with the *simplified* phase-split LPTN for both load cycles are shown in Fig. 6. The difference between the '*hot*' phases and the '*cold*' one is predicted by the models thanks to the split of the winding branch into three different branches. These results confirm the accuracy of the model for the thermal tests performed in ambient air conditions.

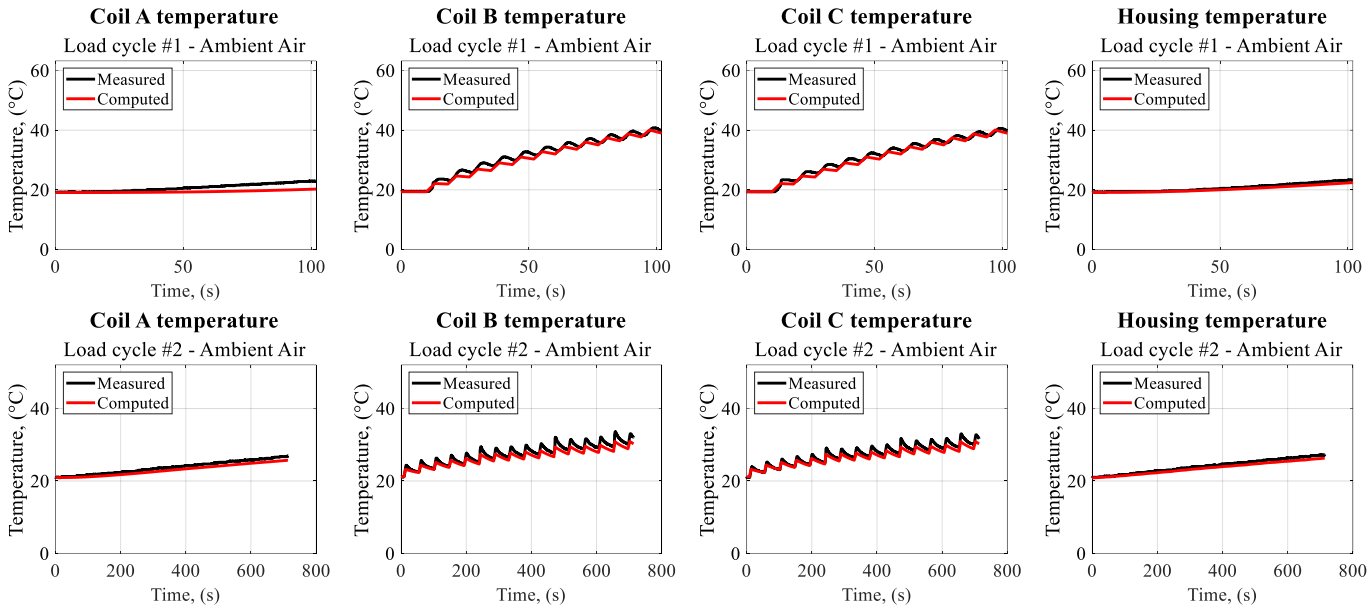

Fig.6 Measured and computed temperatures for the two load cycles in ambient air using the *simplified* phase-split LPTN.

V. Climatic Chamber Tests For The Disk-Shaped Motor

The accuracy of the models must also be verified for the thermal tests performed at an ambient temperature of 120°C to have a prediction of the temperatures closer to the actual operating conditions of the motor inside the BBW system. Therefore, the thermal tests presented in Section II were performed inside the climatic chamber. As an example of the test setup, Fig. 7 shows the *slender* motor inside the climatic chamber. By optimizing on the steady-state and the pulse-current tests, the thermal parameters listed in Table II are obtained, except the parameter R_{hsg} that is measured from the steady-state test.

It can be observed that a lower value of the housing thermal resistance is found from the measurements in the climatic chamber with respect to the value measured in the ambient air. This implies a better heat exchange inside the climatic chamber. By observing the obtained thermal parameters, the conclusion is that, also for the climatic chamber tests, the heat flux mainly reaches the housing through the thermal parameter R_y. Therefore, the *complete* thermal network can be reduced to the *simplified* one, substantially reducing the computational time. The optimized thermal parameters of the *simplified* network are reported in the right column of Table II, and again similar values with respect to the *complete* model are obtained. For these reasons, hereafter, only the results of the *simplified* LPTN are reported.

A. The steady-state and pulse-current thermal tests

In Fig. 8, the measured and computed housing temperatures are depicted. The excellent agreement of the predicted temperatures with the measured profiles confirms the accuracy of the measured R_{hsg}, and of the optimized parameters of both LPTNs. Solid results are obtained for all the pulse-current tests simulated by the phase-split LPTN. For example, Fig. 9 shows the measured and computed temperatures for two of the seven pulse-current tests (60A and 120A).

This confirms the accuracy of model also for the thermal tests performed in the climatic chamber over the thermal tests used to carry out the optimization. However, the ultimate validation must be performed on the load cycle tests inside the climatic chamber.

B. Load cycle thermal tests

At an ambient temperature of 120°C, the electric resistance of the winding differs from its value in ambient air conditions. Therefore, different current values are used to perform the load cycles in the climatic chamber to supply the motors with a similar input power value in ambient air and climatic chamber conditions. Fig.10 reports the obtained temperature for the simulation of the load cycle tests together with the measurements. Also in this case, good results are obtained for the three phases and the housing temperatures. Little discrepancies can be found in the housing temperature prediction; however, the error is less than 3% in the worst case. In conclusion, the model can successfully predict the motor's thermal behaviour in ambient air and climatic chamber with satisfactory accuracy.

Fig.7 The *slender* PM motor inside the climatic chamber.

TABLE II - THERMAL PARAMETERS OF THE PROPOSED LPTNS FOR THE CLIMATIC CHAMBER TESTS.

Parameter	*Complete* LPTN	*Simplified* LPTN
C_1, (J/°C)	67	65
C_2, (J/°C)	$1.488 \cdot 10^7$	
C_3, (J/°C)	622	613
R_x, (°C/W)	20.5	
R_1, (°C/W)	$7.2 \cdot 10^7$	
R_2, (°C/W)	$2.1 \cdot 10^7$	
R_y, (°C/W)	0.89	0.84
R_{hsg}, (°C/W)	1.13	1.13

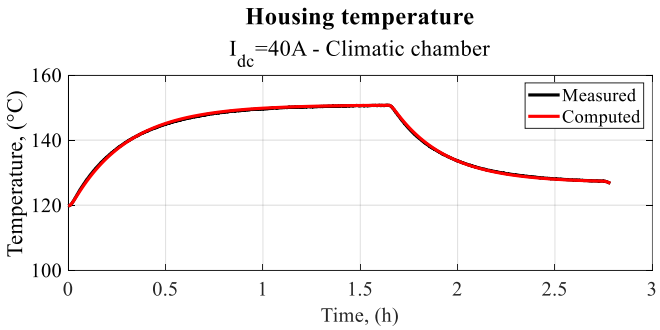

Fig.8 Computed and measured housing temperature for the steady-state test in the climatic chamber.

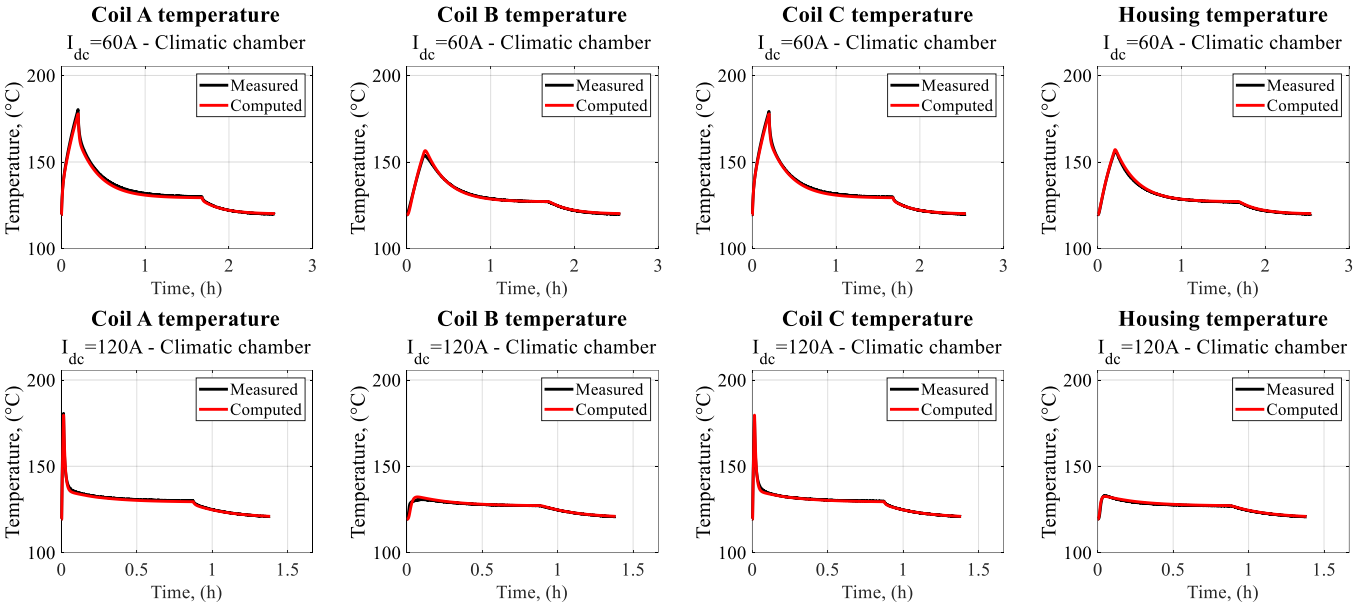

Fig.9 Measured and computed temperatures of the pulse-current test at 60A and 120A for the *simplified* LPTN.

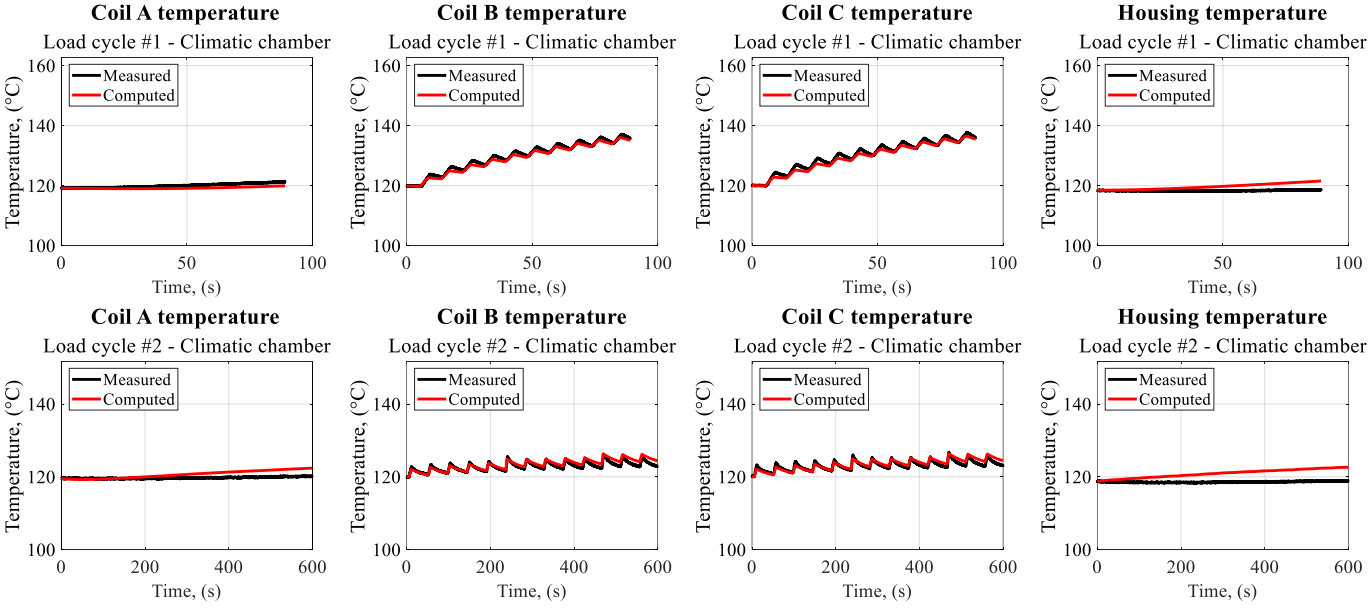

Fig.10 Measured and computed temperatures for the two load cycles in the climatic chamber using the *simplified* phase-split LPTN.

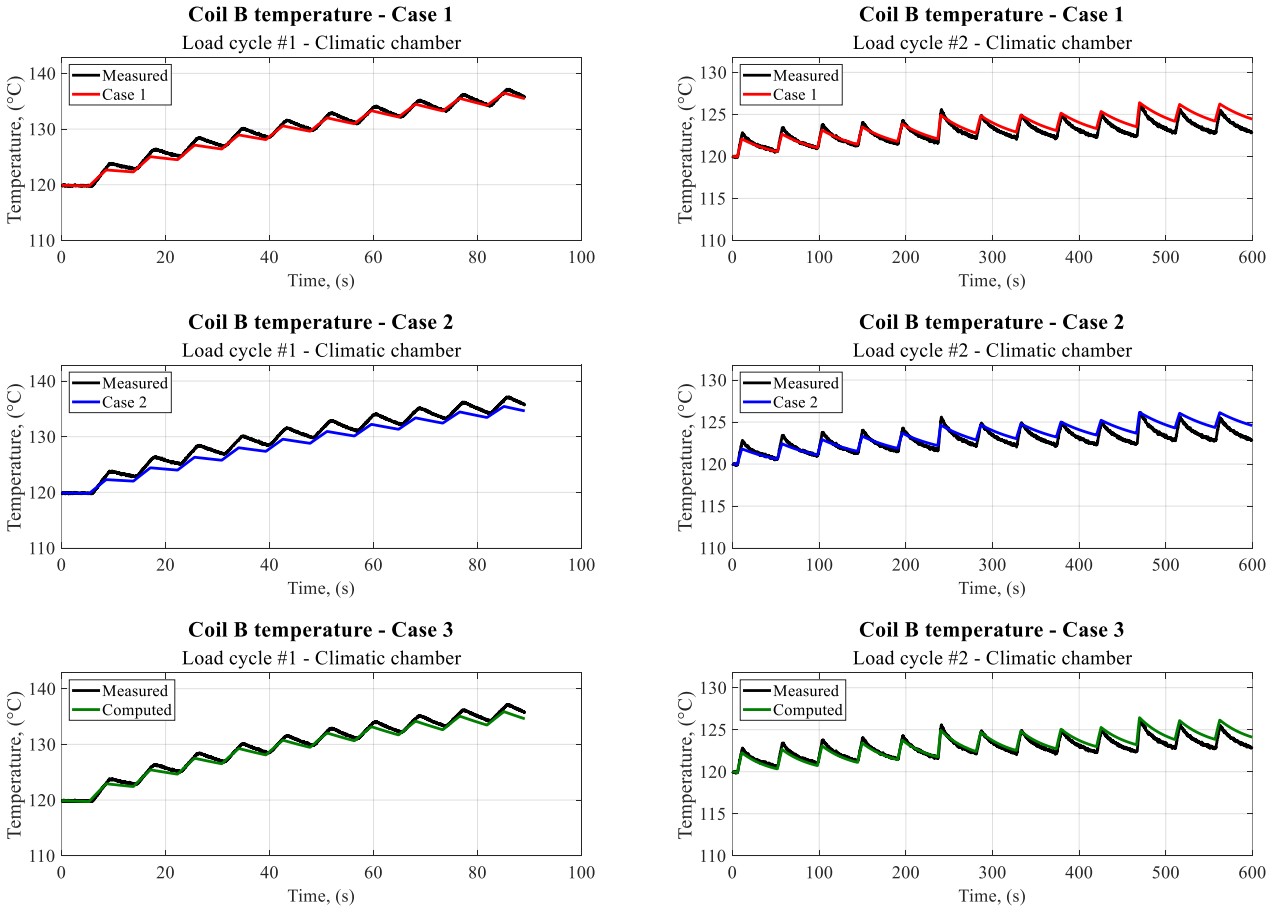

Fig.11 Measured and computed phase B temperature in the three cases of Table III for the two load cycles in the climatic chamber.

VI. Minimization Of The Thermal Tests Requested For The Optimization

At this research stage, the attention has been focused on the minimization of experimental tests needed for correctly calibrating the *simplified* phase-split LPTN for the thermal tests performed in the climatic chamber. In particular, the following cases have been investigated:

1) Calibration based both on the 40A 'steady-state' temperature test and the 120 A pulse-current;
2) Calibration based on the 40A steady-state thermal test only;
3) Calibration based on the 120 A 'pulse-current' only.

The obtained thermal parameters for each case are reported in Table III. The value of the housing-ambient thermal resistance is measured for case 1 and case 2 since the steady-state thermal test is used. For what concerns case 3, the value of R_{hsg} is determined by optimization. The three optimizations led to very similar results. However, a reduced computational time is required to find the thermal parameters since a limited number of tests are managed. The computational time needed by the first case (two tests and three parameters to be found) is around 80s, for the second case around 50s (one test and three parameters to be found) and for the third (one test and four parameters to be found) around 60s.

Fig. 11 reports selected results for the three cases. One of the two '*hot*' phases is reported for the two load cycles. Minor differences can be appreciated among the cases that effectively achieve reliable results. Case 1 requires an additional thermal test with respect of case 2 and case 3, while obtaining very similar thermal parameters. This suggests that the best option for the optimization is between the last two cases.

For case 2, only one standard steady-state test needs to be performed. However, the best performances are reached by the third case, which only relies on one pulse-current test. Indeed, the time duration of the current pulse of the 120A thermal test is around 50s, which is the closest to the short time intervals of the repetitive pulses of the load cycles.

TABLE III - THERMAL PARAMETERS OF THE SIMPLIFIED LPTN IN THE THREE CASES FOR THE CLIMATIC CHAMBER TESTS

	C_1, (J/°C)	C_3, (J/°C)	R_y, (°C/W)	R_{hsg}, (°C/W)
Case 1	65.4	639.2	0.9	1.13
Case 2	75.6	605.4	0.9	1.13
Case 3	57.9	613.6	0.72	1.15

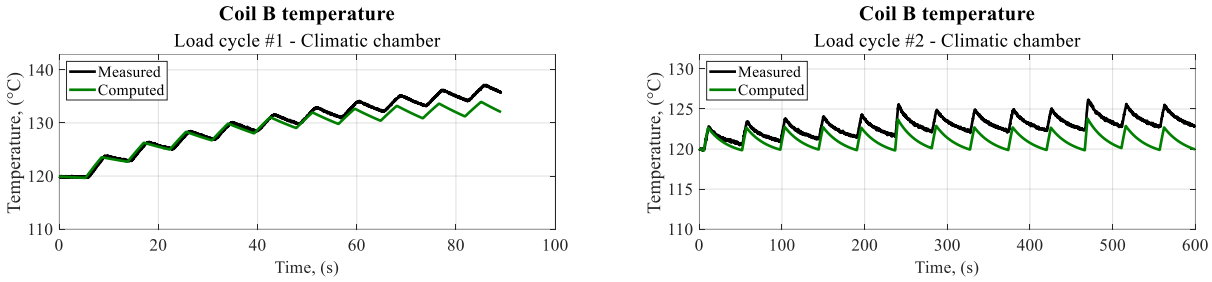

Fig.12 Measured and computed phase B temperature for modified case 3 for the two load cycles in the climatic chamber.

Moreover, the housing-ambient thermal resistance is correctly predicted by the optimization of case 3. Indeed, the cooling with a current of 20A gives sufficient data about the steady-state conditions of the motor. Ultimately, this single test covers the steady-state and the pulse-current information needed for the optimization. Nevertheless, if the current-pulse test is stopped after the pulse duration of 120A, referred as to '*modified case 3*', the phase-split thermal network fails to predict the temperatures, as shown in Fig. 12.

Including the cooling phase, the duration of the pulse-current thermal test is close to the time required to perform the steady-state test. Moreover, higher current levels are necessary for the pulse-current test; thus, adequate lab equipment must be available. In conclusion, case 2 and case 3 are two equally valid options for performing the optimization. However, a sharp simplification of the optimization process has been obtained. Indeed, starting from an optimization based on 1 steady-state test and 8 pulse-current tests with a computational time of almost 6 minutes, an optimization on 1 thermal test with a computational time of approximately 1 minute has been accomplished.

VII. CONCLUSION

The paper presents the thermal analysis of a *disk-shaped* BBW PM motor characterized by an uneven heat distribution during normal operations. The thermal study has been conducted using two different lumped-parameters thermal networks, referred to as *complete* and *simplified* networks, able to model the three phases independently. Several thermal tests have been performed on a motor prototype equipped with thermocouples. The LPTNs have been calibrated by means of the particle swarm optimization technique applied for two different types of thermal tests: steady-state and pulse-current. The optimization allows for obtaining sufficiently accurate thermal parameters. The validation of the models has been carried out on two load tests representative of the actual working conditions of the motor. The obtained results proved that the unconventional heat distribution can be predicted by the thermal models and especially by the *simplified* lumped-parameters thermal network, reducing the required computational time. Moreover, it has been found that the aspect ratio L / D marginally affects the temperature estimations, confirming the accuracy of the model also for disk-shaped machines. Finally, the investigation focused on minimizing the number of thermal tests required by the optimization process. The aim is to lower the computational time and eliminate the burden of performing unnecessary thermal tests.

For the correct model calibration, a steady-state test or a pulse-current test with cooling at a current value different from zero have been pointed out as the best solutions for the optimization. The advantage of the former is that a standard test at low current levels is sufficient to obtain reliable temperature results. The pulse-current-based optimization allows for more accurate results, but proper instruments are needed to perform thermal tests at higher current values.

REFERENCES

[1] Z. Zhu, X. Wang, B. Yan, L. Li, and Q. Wu, 'A Dynamic Decoupling Control Method for PMSM of Brake-by-Wire System Based on Parameters Estimation', *IEEEASME Trans. Mechatron.*, pp. 1–11, 2021.

[2] Q. Shi and L. He, 'A Model Predictive Control Approach for Electro-hydraulic Braking by Wire', *IEEE Trans. Ind. Inform.*, pp. 1–1, 2022.

[3] 'Brembo -Brake By Wire'. https://www.brembo.com/it/BBW/index.html (accessed Jun. 28, 2022).

[4] J. Godbehere, R. Wrobel, D. Drury, and P. H. Mellor, 'Experimentally calibrated thermal stator modelling of AC machines for short-duty transient operation', in *2016 XXII International Conference on Electrical Machines (ICEM)*, Sep. 2016, pp. 1721–1727.

[5] O. Barré and B. Napame, 'The Insulation for Machines Having a High Lifespan Expectancy, Design, Tests and Acceptance Criteria Issues', *Machines*, vol. 5, no. 1, Art. no. 1, Mar. 2017.

[6] C. Sciascera, P. Giangrande, L. Papini, C. Gerada, and M. Galea, 'Analytical Thermal Model for Fast Stator Winding Temperature Prediction', *IEEE Trans. Ind. Electron.*, vol. 64, no. 8, pp. 6116–6126, Aug. 2017.

[7] A. Boglietti, M. Cossale, S. Vaschetto, and T. Dutra, 'Winding Thermal Model for Short-Time Transient: Experimental Validation in Operative Conditions', *IEEE Trans. Ind. Appl.*, vol. 54, no. 2, pp. 1312–1319, Mar. 2018.

[8] F. Graffeo, S. Vaschetto, A. Miotto, F. Carbone, A. Tenconi, and A. Cavagnino, 'Lumped-Parameters Thermal Network of PM Synchronous Machines for Automotive Brake-by-Wire Systems', *Energies*, vol. 14, no. 18, Art. no. 18, Jan. 2021.

[9] D. Wöckinger, G. Bramerdorfer, S. Vaschetto, A. Cavagnino, A. Tenconi, W. Amrhein, F. Jeskey, 'Approaches for Improving Lumped Parameter Thermal Networks for Outer Rotor SPM Machines', in *2021 IEEE Energy Conversion Congress and Exposition (ECCE)*, Oct. 2021, pp. 3821–3828.

[10] Y. Zhu, M. Xiao, K. Lu, Z. Wu, and B. Tao, 'A Simplified Thermal Model and Online Temperature Estimation Method of Permanent Magnet Synchronous Motors', *Appl. Sci.*, vol. 9, no. 15, Art. no. 15, Jan. 2019.

[11] J. Feng, D. Liang, Z. Q. Zhu, S. Guo, Y. Li, and A. Zhao, 'Improved Low-Order Thermal Model for Critical Temperature Estimation of PMSM', *IEEE Trans. Energy Convers.*, vol. 37, no. 1, pp. 413–423, Mar. 2022.

[12] M. Markovic, L. Saunders, and Y. Perriard, 'Determination of the Thermal Convection Coefficient for a Small Electric Motor', in *Conference Record of the 2006 IEEE Industry Applications Conference Forty-First IAS Annual Meeting*, Oct. 2006, vol. 1, pp. 58–61.